Acta Crystallographica Section B
Structural Science
ISSN 0108-7681

New oxybromide cobaltites with layered perovskite-related structures: 18*R*-$Ba_6Co_5BrO_{14}$ and 14*H*-$Ba_7Co_6BrO_{17}$

Matthieu Kauffmann and Pascal Roussel*

UCCS, Equipe Chimie du Solide, CNRS UMR 8181, ENSC Lille – UST Lille, BP 90108, 59652 Villeneuve d'Ascq CEDEX, France

Correspondence e-mail: pascal.roussel@ensc-lille.fr

Received 30 March 2007
Accepted 15 June 2007

Single crystals of the title compounds were prepared by solid–solid reaction using $BaBr_2$ flux at 1373 K. The structures of these two new cobaltites were solved and refined. The two compounds are built from a close-packing of [BaO_3] and [BaOBr] layers with stacking sequences $(c'chhcc')_3$ and $(c'chhhcc')_2$ for the 18*R* and 14*H* structures, respectively, which create Co_3O_{12} trimers or Co_4O_{15} tetramers of face-sharing octahedra connected at their extremities to isolated tetrahedra by corner-sharing. These new materials are strongly related to the 5*H*-$Ba_5Co_5O_{14}$/12*H*-$Ba_{0.9}CoO_{2.6}$ and 10*H*-$Ba_5Co_5ClO_{13}$/6*H*-$Ba_6Co_6ClO_{16}$ materials, with the existence of common blocks. In $Ba_6Co_5BrO_{14}$ and $Ba_7Co_6BrO_{17}$, all the atoms in the vicinity of the [BaOBr] layers are disordered, whereas the rest of the structure is perfectly ordered.

1. Introduction

Transition-metal oxides with layered perovskite-type structure have always been studied by solid-state chemists because of the fascinating properties they often exhibit. In this way, the well known high T_c superconducting cuprates have been widely investigated in the 80s, followed by the colossal magnetoresistive manganites in the 90s. In these two series of materials, the 3*d* transition metal exhibits a wide range of valence states and can adopt several polyhedral configurations. This led to the creation of particularly original structures and as a consequence, spectacular physical properties. More recently, the cobaltite compounds have focused the interest of solid-state researchers because of the peculiarity of the Co ion to adopt several spin configurations, thus providing a supplementary degree of freedom compared with the cuprates and manganite materials. For example, Co^{3+} ions ($3d^6$) in an O_6 octahedral environment may adopt either low-spin (LS, $t_{2g}^6e_g^0$, $S = 0$), intermediate-spin (IS, $t_{2g}^5e_g^1$, $S = 1$) or high-spin (HS, $t_{2g}^4e_g^2$, $S = 2$) configurations (Korotin *et al.*, 1996; Goodenough *et al.*, 1973). The possibility to stabilize several cobalt spin states in this kind of material has been shown to be responsible, for instance, for the metal–insulator transition in the $LnBaCo_2O_{5.5}$ series with a spin-blockade mechanism attributed to the presence of high-spin and low-spin Co^{3+} ions (Maignan *et al.*, 2004). Moreover, the recent discovery of large thermopower properties in metallic Na_xCoO_2 and superconductivity in its hydrated form has strengthened interest in the research in cobaltite materials (Terasaki *et al.*, 1997; Takada *et al.*, 2003).

Layered perovskite-related compounds are made of the periodic stacking along the *c* axis of ideal [AO_3] anionic layers between which the 3*d* transition metal is inserted. In this way,

2*H*-$BaCoO_3$ (Fig. 1*a*; Gushee *et al.*, 1957) is built by the stacking of *h*-[BaO_3] layers (where *h* represents a hexagonal layer, *i.e.* a layer between two layers of the same type, see the convention given by Katz & Ward, 1964) thus leading to the creation of infinite columns of face-sharing octahedra (FSO). Introducing cubic *c*-[BaO_3] layers in the stacking sequence (where *c* represents a layer between two layers of different type) will break the infinite columns of face-sharing octahedra to create strings of face-sharing octahedra connected together through corner-sharing octahedra. For example, the 5*H*-$BaIr_{0.2}Co_{0.8}O_{2.83}$ (Fig. 1*b*; Vente & Battle, 2000) adopts a stacking sequence (*cchhc*) of *h*-[BaO_3] and *c*-[BaO_3] layers creating Co_3O_{12} trimers of face-sharing octahedra connected to each other by corner-sharing octahedra. In the same manner, introducing one supplementary *h*-[BaO_3] layer in the (*cchhc*) sequence would lead to the (*cchhhc*) sequence in which the trimers are replaced by tetramers of face-sharing octahedra Co_4O_{15} (Fig. 1*c*). Furthermore, replacing one ideal *c*-[BaO_3] layer by an oxygen-deficient *c*′-[BaO_2] layer in the previous stacking sequences will create the (*c*′*chhc*) and (*c*′*chhhc*) sequences. In these new sequences, strings of FSO Co_3O_{12} trimers or Co_4O_{15} tetramers are conserved, but the connecting octahedra (corner-shared) are replaced by tetrahedra (isolated). In the cobaltite series, the $Ba_5Co_5O_{14}$ (5*H*; Parras *et al.*, 1995) and $BaCoO_{2.6}$ (12*H*; Jacobson, 1980) compounds adopt, respectively, these original (*c*′*chhc*) and (*c*′*chhhc*) sequences (Figs. 1*d* and *e*). Finally, replacing the oxygen-deficient *c*′-[BaO_2] layer by an *h*′-[BaOCl] layer leads to the (*h*′*chhc*) and (*h*′*chhhc*) sequences. These new sequences are encountered in $Ba_5Co_5ClO_{13}$ (10*H*; Yamaura *et al.*, 2001) and $Ba_6Co_6ClO_{16}$ (6*H*; Tancret *et al.*, 2005), respectively. The replacement of one *c*′-[BaO_2] layer by one *h*′-[BaOCl] layer thus has a structural consequence: the connection of FSO units (Co_3O_{12} trimers or Co_4O_{15} tetramers) is no more realised through isolated tetrahedra but through two corner-shared tetrahedra, leading to the creation of Co_2O_7 dimeric units (Figs. 1*f* and *g*).

In these cobaltite materials, the polyhedra which ensure the connection between FSO trimers Co_3O_{12} or tetramers Co_4O_{15} play a crucial role in the electric and magnetic properties of

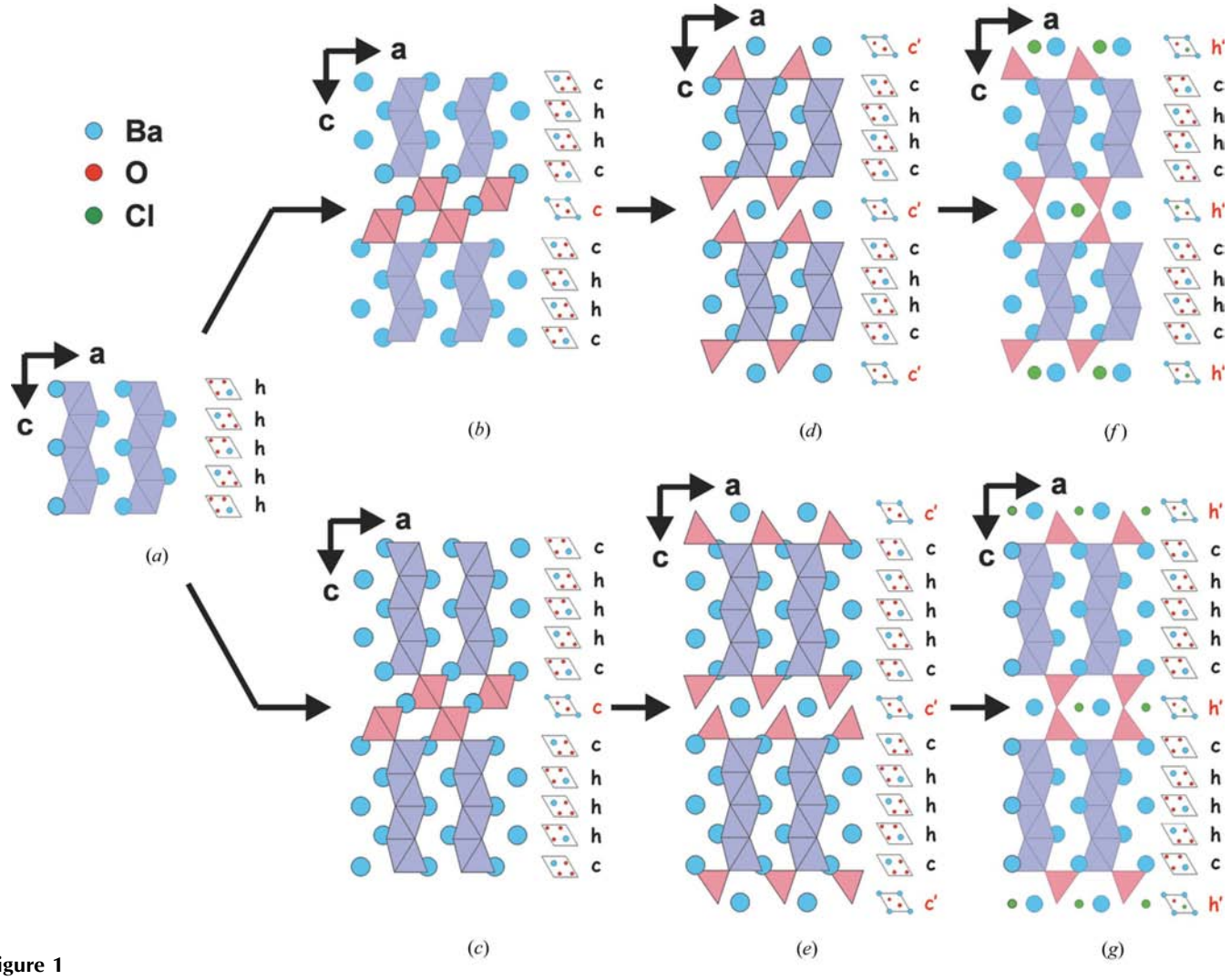

Figure 1
Schematic structures viewed along [010] and stacking sequences of (*a*) 2*H*-$BaCoO_3$ $(h)_2$, (*b*) 5*H*-$BaIr_{0.2}Co_{0.8}O_{2.83}$ (*cchhc*), (*c*) hypothetical structure (*cchhhc*), (*d*) 5*H*-$Ba_5Co_5O_{14}$ (*c*′*chhc*), (*e*) 12*H*-$Ba_{0.9}CoO_{2.6}$ $(c'chhhc)_2$, (*f*) 10*H*-$Ba_5Co_5ClO_{13}$ $(h'chhc)_2$ and (*g*) 6*H*-$Ba_6Co_6ClO_{16}$ (*h*′*chhhc*).

the compounds. For instance, the difference between the resistivity values, at 400 K, for $2H$-$BaCoO_3$, $10H$-$Ba_6Co_6ClO_{16}$ and $12H$-$Ba_{0.9}CoO_{2.6}$ (Maignan *et al.*, 2006) ($\rho \simeq 0.1$, $\rho \simeq 0.1$ and $\rho \simeq 1\ \Omega$ cm, respectively) finds its origin in the connection or disconnection of the chains of polyhedra along the c axis. Indeed, in $BaCoO_3$ and $Ba_6Co_6ClO_{16}$, the c-axis chains of polyhedra are not broken as they are in $Ba_{0.9}CoO_{2.6}$, thus leading to a better conductivity in the $2H$ and the $10H$ structures compared with the $12H$ structure. Moreover, the importance of the interface polyhedra connecting trimer or tetramer units to each other can be illustrated by the magnetic structure of $Ba_6Co_6ClO_{16}$. In this compound, the antiferromagnetic behavior observed below 135 K has been shown to be directly correlated to the Co_2O_7 dimers, since the two tetrahedra forming this unit are strongly antiferromagneticaly coupled (Kauffmann *et al.*, 2006). These two examples show the importance of the interface polyhedra and, consequently, of the layer at the origin of this interface. In the present series, we have seen that this layer can be of three different types: 'ideal' c-[BaO_3], 'lacunar' c'-[BaO_2] or more 'exotic' h'-[BaOCl] layers. Starting from these observations, and in order to modify the structural properties of the interface layer, we tried to synthesize new materials in which the Cl atom of the h'-[BaOCl] layers is substituted by a larger atom having similar chemical affinity, *i.e.* we tried to substitute Cl atoms by Br atoms. With this idea, we succeeded in synthesizing two new oxybromide barium cobaltites, $Ba_6Co_5BrO_{14}$ and $Ba_7Co_6BrO_{17}$. They both contain trimers Co_3O_{12} or tetramers Co_4O_{15} FSO units but the insertion of bromine modifies the interface layer with important structural distortions.

2. Experimental

2.1. Synthesis

Single crystals of $Ba_6Co_5BrO_{14}$ and $Ba_7Co_6BrO_{17}$ were grown using a flux technique. A 3:1:10 molar mixture of BaO_2, Co_3O_4 and $BaBr_2{\cdot}2H_2O$ was well ground in an agate mortar and heated in air at 1373 K for 48 h in an alumina crucible. The mixture was then slowly cooled to 873 at 30 K h^{-1} and the furnace was switched off, allowing gradual cooling to room temperature. After dissolving the excess $BaBr_2$ with hot water, two types of black shiny crystals were extracted from the preparation. Several single crystals were tested on a Bruker X8 APEX2 diffractometer. The needle-shaped single crystals crystallize in a trigonal cell ($a \simeq 5.66$ and $c \simeq 43.17$ Å) and correspond to the new $Ba_6Co_5BrO_{14}$ material. The hexagonal plate-like ones give a hexagonal cell ($a \simeq 5.66$ and $c \simeq 33.57$ Å) and correspond to the new $Ba_7Co_6BrO_{17}$ compound.

Several single crystals were analyzed by energy-dispersive X-ray spectroscopy on a Jeol JSM-5300 scanning microscope equipped with an IMIX system from Princeton Gamma Technology. Measurements revealed the presence of all elements introduced in the preparation: barium, cobalt, bromine and oxygen. Semi-quantitative analysis realised on several points of the crystals confirmed the formula of each compound.

Synthesis of polycrystalline samples of both compounds were conducted using $BaCO_3$, Co_3O_4 and $BaBr_2{\cdot}2H_2O$ as precursors. Experiments show that the obtained products strongly depend on the reaction temperature. A pure powder of $Ba_7Co_6BrO_{17}$ was synthesized by solid-state reaction between the precursors in the stoichiometric ratio 13:4:1, at 1173 K over 72 h. Several intermediate regrindings were necessary in order to homogenize the mixture. High-temperature X-ray diffraction analysis of $Ba_7Co_6BrO_{17}$ performed on a Bruker D8 diffractometer reveals a phase transformation at 1263 K, following the reaction below.

$$14H\text{-}Ba_7Co_6BrO_{17} \rightarrow 18R\text{-}Ba_6Co_5BrO_{14} + BaCoO_{2.23} + 0.385O_2$$

Taking advantage of this phase transformation, we succeeded in obtaining $Ba_6Co_5BrO_{14}$ as a pure phase following this protocol: first a 33:10:3 molar mixture of $BaCO_3$, Co_3O_4 and $BaBr_2{\cdot}2H_2O$ was preheated at 1173 K over 48 h with several regrindings. The mixture was then heated at 1263 K for 72 h, ground several times and then quenched to room temperature. To summarize the results of HTXRD (high-temperature X-ray diffraction) analysis, $Ba_7Co_6BrO_{17}$ can only be formed at low temperature (1173 K), whereas $Ba_6Co_5BrO_{14}$ is obtained at high temperature (1263 K). Note that during the single-crystals synthesis, the two phases have been obtained in the same batch, probably due to the particular conditions involved by the $BaBr_2$ flux. At higher temperature (> 1273 K), the $18R$-$Ba_6Co_5BrO_{14}$ and $BaCoO_{2.23}$ mixture is totally decomposed into $BaCoO_{2.23}$ (Strauss *et al.*, 1951), which seems to be the only stable phase at very high temperature (as commonly observed in the cobaltite-related materials). The purity of $Ba_6Co_5BrO_{14}$ and $Ba_7Co_6BrO_{17}$ powders was checked by X-ray diffraction using a Huber G670 diffractometer with Guinier geometry, equipped with front-monochromator producing Cu $K\alpha_1$ radiation.

2.2. Crystal structure determination

Single-crystal diffraction data of $Ba_6Co_5BrO_{14}$ and $Ba_7Co_6BrO_{17}$ were collected on a Bruker X8 APEX2 diffractometer using Mo $K\alpha$ radiation (λ = 0.71073 Å) selected by a graphite monochromator. The ω-scan angle and the D_x parameter were fixed for both compounds to 0.5° per frame and 40 mm, because of the high quality of the selected crystals. An acquisition time of 20 s per frame was used. The diffracted intensities were collected up to 2θ = 87.50° with 13 868 reflections and a redundancy of 11.26 in point group $\bar{3}m$ for $Ba_6Co_5BrO_{14}$ and 2θ = 79.72° with 11 909 reflections and a redundancy of 10.15 in $6/mmm$ for $Ba_7Co_6BrO_{17}$. After data collection, the intensity data were integrated and corrected for Lorentz, polarization and background effects using the *SAINT*7.12 software (Bruker Analytical X-ray Instruments Inc., 2004). The *SADABS*2006/1 program (Sheldrick, 2006) was used to correct absorption effects using a redundancy

Table 1
Crystal data, intensity collection and structure refinement parameters for 14*H*-$Ba_7Co_6BrO_{17}$ and 18*R*-$Ba_6Co_5BrO_{14}$.

	$Ba_7Co_6BrO_{17}$	$Ba_6Co_5BrO_{14}$
Crystal data		
Chemical formula	$Ba_7BrCo_6O_{17}$	$Ba_6BrCo_5O_{14}$
M_r	1666.9	1422.6
Cell setting, space group	Hexagonal, $P6_3/mmc$	Trigonal, $R\bar{3}m$
Temperature (K)	293	293
a, bc (Å)	5.66110 (10), 5.66110 (10), 33.5672 (8)	5.6578 (3), 5.6578 (3), 43.166 (4)
V (Å^3)	931.64 (3)	1196.65 (14)
Z	2	3
D_x (Mg m^{-3})	5.940	5.920
Radiation type	Mo $K\alpha$	Mo $K\alpha$
μ (mm^{-1})	21.93	22.16
Crystal form, colour	Hexagonal platelets, black	Hexagonal platelets, black
Crystal size (mm)	0.12 × 0.09 × 0.06	0.13 × 0.10 × 0.06
Data collection		
Diffractometer	Bruker APEX II, CCD 4K	Bruker APEX II, CCD 4K
Data collection method	φ and ω scans	φ and ω scans
Absorption correction	Multiscan	Multiscan
T_{min}	0.139	0.128
T_{max}	0.518	0.265
No. of measured, independent and observed reflections	11 909, 1158, 1045	13 868, 1232, 1117
Criterion for observed reflections	$I > 3\sigma(I)$	$I > 3\sigma(I)$
R_{int}	0.045	0.045
θ_{max} (°)	39.9	43.8
Refinement		
Refinement on	F	F
$R[F^2 > 2\sigma(F^2)]$, $wR(F^2)$, S	0.048, 0.066, 4.70	0.032, 0.047, 3.86
Final R indices (R, wR) for MEM	0.0204/0.0160	0.0161/0.0162
No. of reflections	1158	1232
No. of parameters	53	46
Weighting scheme	Based on measured s.u.s $w = 1/\sigma^2(F)$	Based on measured s.u.s $w = 1/\sigma^2(F)$
$(\Delta/\sigma)_{max}$	0.001	<0.0001
$\Delta\rho_{max}$, $\Delta\rho_{min}$ (e Å^{-3})	7.98, −5.50	4.36, −4.12
Extinction method	B-C type 1 Gaussian isotropic (Becker & Coppens, 1974)	B-C type 1 Gaussian isotropic (Becker & Coppens, 1974)
Extinction coefficient	0.028 (8)	0.023 (5)

Computer programs used: *JANA*2000 (Petricek *et al.*, 2005).

algorithm. Details of the data collection and refinements are given in Table 1. Indexing of diffraction data yielded trigonal/hexagonal unit cells with the parameters a = 5.6578 (3) and c = 43.166 (4) Å for 18*R*-$Ba_6Co_5BrO_{14}$ and a = 5.6611 (1) and c = 33.5672 (8) Å for 14*H*-$Ba_7Co_6BrO_{17}$.

Crystal structures were determined for both compounds by direct methods using the *SIR*97 program (Altomare *et al.*, 1997), which readily established the heavy-atom positions (Ba, Co and Br). O-atom positions were found by difference-Fourier map calculations. Anisotropic displacement parameters were refined for all atoms in the last cycles of refinement. Full-matrix least-squares structure refinements against F were carried out using the *JANA*2000 program (Petricek *et al.*, 2005). The refinements led to the residual values R_{all} = 0.0534 and wR_{all} = 0.0660 for $Ba_7Co_6BrO_{17}$ and R_{all} = 0.0342 and wR_{all} = 0.0470 for $Ba_6Co_5BrO_{14}$.

As already reported in one of our previous papers (Kauffmann *et al.*, 2007), the introduction of Br atoms in this type of layered compounds can lead to structural disorder. We thus undertook a maximum entropy method (MEM) analysis of the diffraction data collected on $Ba_6Co_5BrO_{14}$ and $Ba_7Co_6BrO_{17}$. MEM is a model-free method which is used to calculate accurate electron densities in solids using experimentally phased structure factors as input. This method has been proved to be particularly suited to determine the structural aspects of disorder and anharmonic vibrations (Bagautdinov *et al.*, 1998). To calculate the precise electron-density distribution, the MEM analysis was carried out using the computer program *BayMEM* (Palatinus & van Smaalen, 2005). The total number of electrons in the unit cell has been fixed to $F(000)$ values (1854 and 1450 e$^-$ for $Ba_6Co_5BrO_{14}$ and $Ba_7Co_6BrO_{17}$, respectively) and the unit cell was divided in a grid of 72 × 72 × 486 pixels to ensure a good resolution (better than 0.1 Å for the two studied compounds). All calculations were performed with an initial flat electron density with all the independent reflections. The reliability factor of the MEM, $R_{MEM} = \sum |F_{obs} - F_{MEM}| / \sum |F_{obs}|$, is given in Table 1 ($F_{obs}$ is obtained by the structural refinement and F_{MEM} is the structure factor calculated from the electron density obtained by the MEM).

3. Results and discussion

The atomic coordinates and anisotropic displacement parameters for $Ba_6Co_5BrO_{14}$ and $Ba_7Co_6BrO_{17}$ deduced from the single-crystal refinements are in the supplementary material.[1] Views of the structures in projection along [010] are given in Fig. 2. Crystal structures of both compounds are very close to the cobaltites presented in §1. They are built by the stacking along the c axis of 'classical' [BaO_3] and new 'original'

[1] Supplementary data for this paper are available from the IUCr electronic archives (Reference: BP5003). Services for accessing these data are described at the back of the journal.

Table 2
Selected bond distances (Å) in $Ba_6Co_5BrO_{14}$ and $Ba_7Co_6BrO_{17}$.

In both materials, Co1 and Co2 atoms are octahedral, whereas Co3 atoms are tetrahedral. Average distances are given in bold.

$Ba_6Co_5BrO_{14}$		$Ba_7Co_6BrO_{17}$	
Co1—O1	1.939 (2) × 3	Co1—O1	1.958 (5) × 3
Co1—O2	1.918 (2) × 3	Co1—O2	1.905 (4) × 3
Co1—O	**1.928 (3)**	**Co1—O**	**1.931 (4)**
Co2—O2	**1.892 (2) × 6**	Co2—O2	1.876 (4) × 3
		Co2—O3	1.895 (4) × 3
Co3—O1	1.839 (2) × 3	**Co2—O**	1.885 (4)
Co3—O3	1.759 (9) × 1		
Co3—O	1.819 (2)	Co3—O3	1.817 (5) × 3
		Co3—O4	1.81 (2) × 1
		Co3—O	**1.815 (5)**
Co1—Co2	2.4799 (9)		
		Co1—Co2	2.465 (2)
		Co2—Co2	2.399 (2)

[BaOBr] layers. $Ba_6Co_5BrO_{14}$ can be derived from 5*H*-$Ba_5Co_5O_{14}$ (Parras *et al.*, 1995) by replacing the *c*′-[BaO_2] layer by two *c*′-[BaOBr] layers, creating an 18-layers stacking sequence (*c*′*chhcc*′)$_3$. In this structure, the Co_3O_{12} trimeric units created by the (*chhc*) sequence are connected at their extremities to a single isolated tetrahedron. As in $Ba_5Co_5O_{14}$, the blocks of three octahedra and two tetrahedra are clearly disconnected from each other but the distance between two tetrahedral cobalts is substantially longer in the bromide 18*R* structure [6.591 (1) Å] compared with the oxide 5*H* structure [4.66 (1) Å], owing to the insertion of two *c*-layers instead of one. In the same manner, $Ba_7Co_6BrO_{17}$ can be derived from 12*H*-$BaCoO_{2.6}$ (Jacobson, 1980) by replacing the *c*′-[BaO_2] layer by two *c*′-[BaOBr] layers, creating the 14-layers stacking sequence (*c*′*chhhcc*′)$_2$ with tetrameric units of face-sharing octahedra Co_4O_{15}. Projections of both structures along the [110] direction show the existence of a triangular network built by the octahedra tetramers or trimers which are linked to each other through tetrahedra located at the centre of each triangle. Note that $Ba_7Co_6BrO_{17}$ is related to $Ba_6Co_5BrO_{14}$ by removing one *h*-[BaO_3] layer and one Co atom. This fact may explain the phase transition which occurs at high temperature with the transformation of 14*H*-$Ba_7Co_6BrO_{17}$ into 18*R*-$Ba_6Co_5BrO_{14}$ and $BaCoO_{2.23}$.

The calculated average cobalt oxidation state of +3.40 in $Ba_6Co_5BrO_{14}$ can be explained by a valence ordered-sites model with Co^{4+} in tetrahedral (Co3) and Co^{3+} in octahedral sites (Co1 and Co2). If charge ordering were taking place such that the Co^{4+} ions were predominantly present on tetrahedral sites, they would expect a significantly shorter average Co—O bond than the conventional tetrahedral Co^{2+}—O bond (1.928 Å in the spinel Co_3O_4 or 1.92–1.98 Å in $YbBaCo_4O_{7-\delta}$). As shown in Table 2, the short Co3—O bond distance of 1.819 (4) Å confirms the charge-ordering model proposed, in good agreement with the smaller ionic radius for Co^{4+}, leading to the formula $Ba_6Co_3^{3+}Co_2^{4+}BrO_{14}$. This kind of charge ordering has already been observed in the $Ba_5Co_5FO_{13}$ material, for example (Ehora *et al.*, 2007). In $Ba_7Co_6BrO_{17}$, the average Co3—O distance of 1.815 (5) Å strongly suggests a Co^{4+} ordering in tetrahedral sites, as in $Ba_6Co_5BrO_{14}$. This would lead to a mixed octahedral Co^{3+}/Co^{4+} partition, as observed for instance in the $BaCoO_{3-\delta}$ series. Nevertheless, we cannot exclude the presence of oxygen vacancies in this kind of compound, which can reduce the average cobalt oxidation state

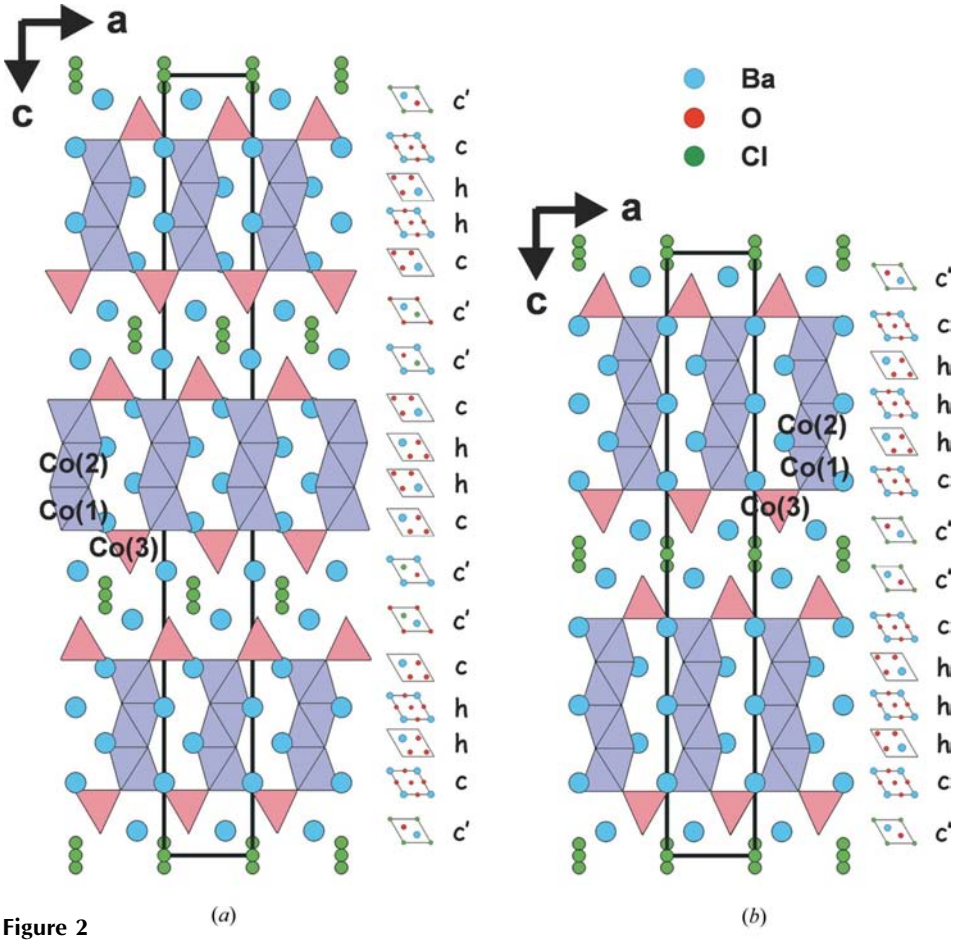

Figure 2
Schematic crystal structures of (*a*) 18*R*-$Ba_6Co_5BrO_{14}$ and (*b*) 14*H*-$Ba_7Co_6BrO_{17}$ viewed along [010]. Purple or pink polygons represent octahedral or tetrahedral Co atoms, respectively. For clarity, only an ideal model is drawn, without splitting of any disordered atoms.

from +3.5 to 3.33, for a final formula $Ba_7Co_4^{3+}Co_2^{4+}BrO_{16.5}$, as observed for example in $Ba_6Co_6ClO_{16}$ (Kauffmann *et al.*, 2006). In $Ba_6Co_6ClO_{16}$, both redox chemical analysis and neutron diffraction experiments have shown the existence of lacunar [BaO_3] layers, leading to the true formula $Ba_6Co_6ClO_{15.5}$ with a tetrahedral Co^{4+}/octahedral Co^{3+} partition. In $Ba_7Co_6BrO_{17}$, the shorter average Co2—O bond length of 1.885 (5) Å compared with the Co1—O bond distance of 1.931 (5) Å is also consistent with the presence of oxygen vacancies, leading to a lower average coordination of the Co2 sites. The valence-ordered site model with Co^{4+} in tetrahedral sites and Co^{3+} in octahedral sites seems to be the more realistic one for this compound.

The two-dimensional contour electron-density (ED) images are shown in Fig. 3 in the region of the [BaOBr] layers. These images show that for both compounds, Ba, Br and O atoms participating in the [BaOBr] layers are clearly disordered. In $Ba_6Co_5BrO_{14}$, the Ba3 site displays a triangular shape indicating a small splitting over the threefold axis centred on a 6(*c*) position (Fig. 3*a*). Therefore, this atom has been refined on the position 18(*h*) with an occupancy of 0.333. In the same manner, the Ba4 atom in $Ba_7Co_6BrO_{17}$ has been split from its original 4(*f*) site to a 12(*k*) position occupied at 0.333. O atoms of this special [BaOBr] layer [O3 in $Ba_6Co_5BrO_{14}$ (Fig. 3*b*) and O4 in $Ba_7Co_6BrO_{17}$] were also split from their threefold axis to explain the electron density calculated by MEM. In $Ba_5Co_5FO_{13}$ or $Ba_6Co_6FO_{16}$/$Ba_6Co_6ClO_{16}$, this kind of split has also been observed with the same kind of disorder on the central O atom of the tetrahedral cobalt. Disorder found for Br atoms is more complex. Indeed, in both materials, MEM electron density images show that bromine is not localized at a point but distributed on two sites to form a kind of electron density column (Fig. 3*c*). To model this disorder, we split bromine on sites 6(*c*) and 3(*a*) in $Ba_6Co_5BrO_{14}$ with occupancies of 0.23 (3) and 0.55 (5), respectively. The occupancy parameters of the Br ions were constrained to unity to fulfil

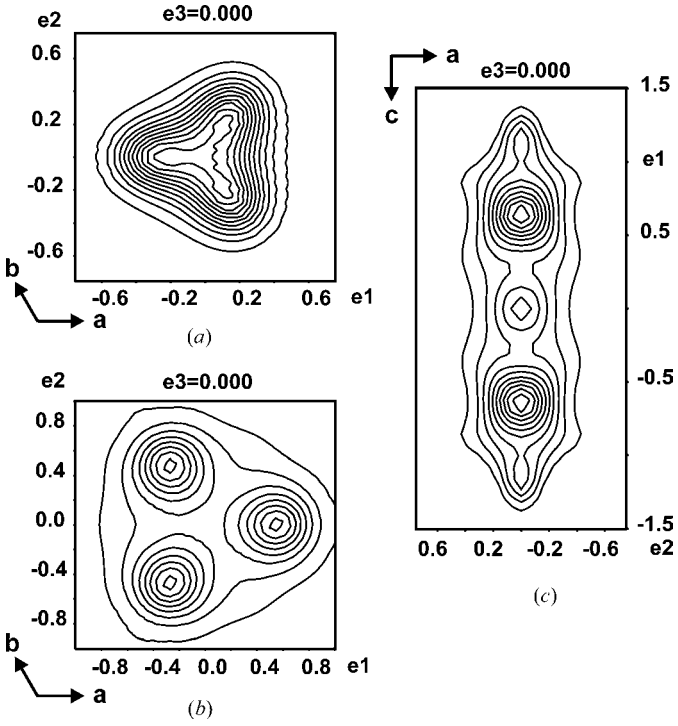

Figure 3
Two-dimensional contour plot of the electron density calculated by MEM for (*a*) Ba3, (*b*) O3 and (*c*) Br for the 18*R*-$Ba_6Co_5BrO_{14}$ compound. Plots of the electron density are very similar for 14*H*-$Ba_7Co_6BrO_{17}$.

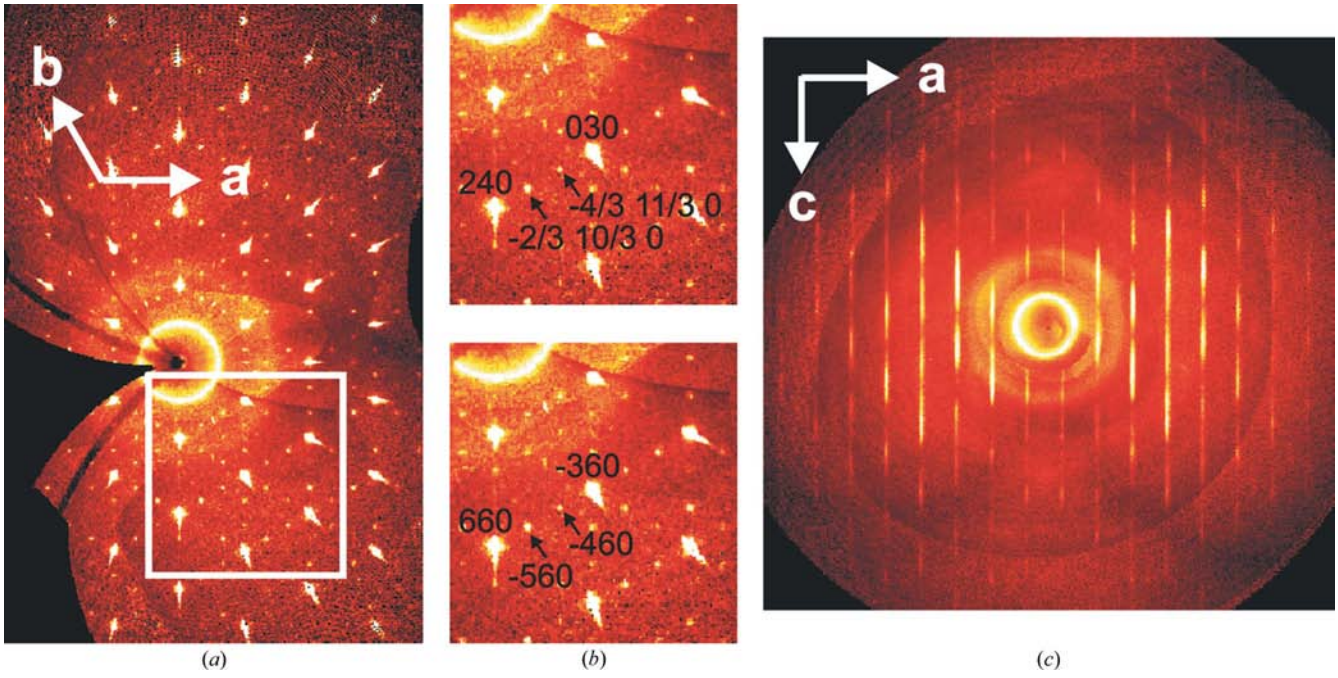

Figure 4
Precession images calculated from single-crystal X-ray diffraction data: (*a*) (*hk*0) plane, (*b*) zoom of the (*hk*0) plane and (*c*) ($\frac{1}{3}kl$) plane.

the chemical composition $Ba_6Co_5BrO_{14}$. In the same manner, bromine was split in $Ba_7Co_6BrO_{17}$ with occupancies of 0.44 (1) and 0.13 (3) on 4(*e*) and 2(*a*) sites. Apart from these special positions, the electron-density distribution of other atoms in the structures was in good agreement with harmonic shapes. In summary, all the atoms in the vicinity of the [BaOBr] layers are disordered, whereas the rest of the structure is perfectly ordered.

The use of an automatic single-crystal diffractometer with a very sensitive two-dimensional CCD detector has opened new perspectives in crystal-structure analysis. Indeed, data collection performed with such a CCD diffractometer yields an enormous amount of information on the diffraction pattern in the whole reciprocal space. The diffraction intensities between the reciprocal lattice points (the so-called Bragg spots), usually neglected in routine crystal-structure analysis, can contain information about the short-range order in disordered crystal structures. We used this ability of the X8 Apex2 software to reconstruct precession images to search more information on the data collected for the two title compounds. In the first step, we have reconstructed 'classical' planes, *i.e.* (*hk*0), (*hk*1), (*h*0*l*), (*h*1*l*), (0*kl*) and (1*kl*) layers. Fig. 4(*a*) gives, as an example, the (*hk*0) layer reconstructed for 14*H*-$Ba_7Co_6BrO_{17}$. We can clearly see that additional spots are visible, see zoom in Fig. 4(*b*), in the commensurate position ($\frac{1}{3}\frac{1}{3}$ 0). We then tried to integrate the intensities in a supercell [a = 9.8050 (1) and c = 33.5672 (8) Å] deduced from the previous one using the matrix relation

$$\begin{pmatrix} 1 & 1 & 0 \\ -1 & 2 & 0 \\ 0 & 0 & 1 \end{pmatrix}$$

(see the indexation of the Miller indices in this new cell in the lower part of Fig. 4*b*). Unfortunately, the integration process was not converging. We then undertook the reconstruction of precession images through these supplementary spots, *i.e.* ($\frac{1}{3}kl$) ($\frac{2}{3}kl$) ($h\frac{1}{3}l$) and ($h\frac{2}{3}l$) planes. An example of a typical reconstructed plane is given in Fig. 4(*c*): in fact, what we thought to be additional Bragg spots are diffuse streaks aligned along the [001] direction. It is quite clear that the intersection of such streaks in the (*hk*0) plane give the appearance of spots. The evidence of these diffuse strings is reinforcing the fact that these structures are not completely ordered. Indeed, such phenomena have already been observed in the short-range order of stacking layer structures (Welberry, 2001; Proffen & Neder, 1997) and they are consistent with the MEM analysis.

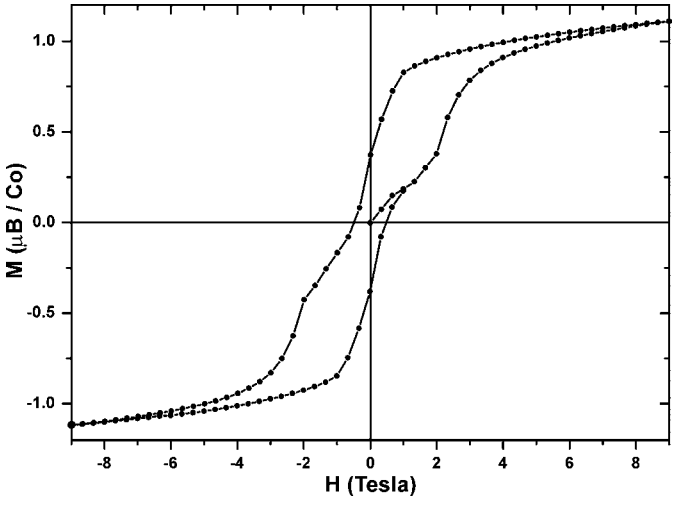

Figure 5
M versus H curve of the $Ba_7Co_6BrO_{17}$ compound at 5 K.

Measurements of the magnetic susceptibility (χ) against temperature (T) have been performed on pure polycrystalline powder for $Ba_6Co_5BrO_{14}$ and $Ba_7Co_6BrO_{17}$ under applied magnetic fields of 0.1 and 1 T. The magnetic behaviors of both compounds are similar with the existence of a first transition at $\sim$ 60 K and a second one below 30 K. $Ba_6Co_5BrO_{14}$ and $Ba_7Co_6BrO_{17}$ are paramagnetic above 60 K: $\chi^{-1} = f(T)$ data were fitted to the Curie–Weiss law leading to the values $p_{\rm eff}$ = 3.57 μB per Co and θ = 45 K for the 18*R* structure and $p_{\rm eff}$ = 3.12 μB per Co and θ = 55 K for the 14*H* structure. No significant difference was found for the effective moments calculated under an applied field of 0.1 T and those calculated for a field of 1 T. These paramagnetic effective moments can be explained by assuming Co^{3+} S = 1 and Co^{4+} S = 3/2, *i.e.* Co atoms at the intermediate spin state (giving the theoretical values $p_{\rm eff}$ = 3.25 μB per Co and $p_{\rm eff}$ = 3.18 μB per Co for $Ba_6Co_5BrO_{14}$ and $Ba_7Co_6BrO_{17}$, respectively, considering the spin-only approximation). The values of $p_{\rm eff}$ and θ deduced from the Curie–Weiss law for both compounds are very similar to those calculated for 12*H*-$Ba_{0.9}CoO_{2.6}$ (Maignan *et al.*, 2006; $p_{\rm eff}$ = 3.7 μB per Co and θ = 50 K) and for 5*H*-$Ba_5Co_5O_{14}$ (Boulahya *et al.*, 2005; $p_{\rm eff}$ = 3.9 μB per Co and θ = 47.9 K), confirming the strong relationship between the four structures. For $Ba_6Co_5BrO_{14}$ and $Ba_7Co_6BrO_{17}$, the positive θ values indicate important ferromagnetic exchanges among the structures, in good agreement with the hysteretic character of the *M versus H* curves (see for example on Fig. 5 the magnetic field dependence of the magnetization at 5 K for $Ba_7Co_6BrO_{17}$). However, the curves show interesting multi-step magnetizations which reveal that the magnetic behaviours of these materials are complex and fascinating, and they are therefore under further investigation. Neutron diffraction studies are planned to establish the magnetic structure and will be published in a further work.

4. Conclusions

To summarize the main findings of the work presented here, we have determined the structures of two cobaltites closely related to previously reported materials with the existence of common blocks. They are built from a close-packing of [BaO_3] and [BaOBr] layers with stacking sequences $(c'chhcc')_3$ and $(c'chhhcc')_2$ for 18*R*-$Ba_6Co_5BrO_{14}$ and 14*H*-$Ba_7Co_6BrO_{17}$ structures, respectively, which create Co_3O_{12} trimers or Co_4O_{15} tetramers of face-sharing octahedra connected to isolated tetrahedra by corner-sharing. The role of the bromine seems to be of particular interest for the modification of the structures: all the atoms in the vicinity of the [BaOBr] layers

are disordered, whereas the rest of the structure is perfectly ordered.

M. K. is indebted to 'CNRS' and 'Région Nord Pas-de-Calais' for financial support. The 'Fonds Européen de Développement Régional (FEDER)', 'CNRS', 'Région Nord Pas-de-Calais' and 'Ministère de l'Education Nationale, de l'Enseignement Supérieur et de la Recherche' are acknowledged for funding for the X-ray diffractometers. The authors are grateful to Dr Olivier Mentré and Professor Francis Abraham for stimulating discussions, valuable advice and for the critical reading of this manuscript.

References

Altomare, A., Burla, M. C., Camalli, M., Cascarano, G., Giacovazzo, C., Guagliardi, A., Moliterni, A. G. G., Polidori, G. & Spagna, R. (1997). *SIR*97. Bari, Rome, Italy.

Bagautdinov, B., Luedecke, J., Schneider, M. & van Smaalen, S. (1998). *Acta Cryst.* B**54**, 626–634.

Becker, P. J. & Coppens, P. (1974). *Acta Cryst.* A**30**, 129–147.

Boulahya, K., Parras, M., Gonzales-Calbet, J. M., Amador, U., Martinez, J. L., Tissen, V. & Fernandez-Diaz, M. T. (2005). *Phys. Rev. B*, **71**, 14402.

Bruker Analytical X-ray Instruments Inc. (2004). *SAINT*+, Version 7.12. Bruker Analytical X-ray Instruments Inc., Madison, Wisconsin, USA.

Ehora, G., Renard, C., Daviero-Minaud, S. & Mentré, O. (2007). *Chem. Mater.* **19**, 2924–2926.

Goodenough, J. B., Demazeau, G., Pouchard, M. & Hagenmuller, P. (1973). *J. Solid State Chem.* **8**, 325–330.

Gushee, B. E., Katz, L. & Ward, R. (1957). *J. Am. Chem. Soc.* **79**, 5601–5603.

Jacobson, A. J. (1980). *J. Solid State Chem.* **35**, 334–340.

Katz, L. & Ward, R. (1964). *Inorg. Chem.* **3**, 205–211.

Kauffmann, M., Mentré, O., Legris, A., Tancret, N., Abraham, F. & Roussel, P. (2006). *Chem. Phys. Lett.* **432**, 88–93.

Kauffmann, M., Tancret, N., Abraham, F. & Roussel, P. (2007). *Solid State Sci.* Accepted for publication.

Korotin, M., Ezhov, S., Solovyev, I., Anisimov, V., Khomskii, D. & Sawatzky, G. A. (1996). *Phys. Rev. B*, **54**, 5309–5316.

Maignan, A., Caignaert, V., Raveau, B., Khomskii, D. & Sawatzky, G. A. (2004). *Phys. Rev. Lett.* **93**, 026401.

Maignan, A., Hébert, S., Pelloquin, D. & Pralong, V. (2006). *J. Solid State Chem.* **179**, 1852–1856.

Palatinus, L. & van Smaalen, S. (2005), *BAYMEM*. University of Bayreuth, Germany.

Parras, M., Varela, A., Seehofer, H. & Gonzalez-Calbet, J. M. (1995). *J. Solid State Chem.* **120**, 327–331.

Petricek, V., Dusek, M. & Palatinus, L. (2005). *JANA*2000. Praha, Czech Republic.

Proffen, Th. & Neder, R. B. (1997). *J. Appl. Cryst.* **30**, 171–175.

Sheldrick, G. M. (2006). *SADABS*, Version 2006/1. University of Göttingen, Germany.

Strauss, S. W., Fankuchen, I. & Ward, R. (1951). *J. Am. Chem. Soc.* **73**, 5084–5086.

Takada, K., Sakurai, H., Takayama-Muromachi, E., Izumi, F., Dilanian, R. A. & Sasaki, T. (2003). *Nature*, **422**, 53–55.

Tancret, N., Roussel, P. & Abraham, F. (2005). *J. Solid State Chem.* **178**, 3066–3073.

Terasaki, I., Sasago, Y. & Uchinokura, K. (1997). *Phys. Rev. B*, **56**, R12685.

Vente, J. F. & Battle, P. D. (2000). *J. Solid State Chem.* **152**, 361–373.

Welberry, T. R. (2001). *Acta Cryst.* A**57**, 244–255.

Yamaura, K., Young, P. D., Siegrist, T., Besnard, C., Svensson, C., Liu, Y. & Cava, R. J. (2001). *J. Solid State Chem.* **158**, 175–179.